AGU PUBLICATIONS

JGR

Journal of Geophysical Research: Space Physics

RESEARCH ARTICLE
10.1002/2016JA022861

Key Points:
- Merging occurs when one EPB tilts and meets the channel of adjacent EPB
- Secondary instabilities growing on the wall of an EPB might merge with nearby EPB
- Two EPBs merge when the leading EPB slows down and trailing EPB catches up

Correspondence to:
V. L. Narayanan,
narayananvlwins@gmail.com

Citation:
Narayanan, V. L., S. Gurubaran, and K. Shiokawa (2016), Direct observational evidence for the merging of equatorial plasma bubbles, *J. Geophys. Res. Space Physics*, *121*, doi:10.1002/2016JA022861.

Received 22 DEC 2015
Accepted 18 JUL 2016
Accepted article online 19 JUL 2016

Direct observational evidence for the merging of equatorial plasma bubbles

V. L. Narayanan[1], S. Gurubaran[2], and K. Shiokawa[3]

[1]Indian Institute of Science Education and Research Mohali, S.A.S. Nagar, India, [2]Indian Institute of Geomagnetism, Navi Mumbai, India, [3]Institute for Space-Earth Environmental Research, Nagoya University, Nagoya, Japan

Abstract In this work we present direct ground-based observational evidence for the merging of individual equatorial plasma bubbles (EPBs) obtained through the imaging of OI 630.0 nm airglow. Three potential mechanisms have been identified: (1) One of the EPBs tilts and reaches location of the adjacent growing EPB finally merging with it. (2) Some of the branches of an EPB arising from secondary instabilities reach out to adjacent EPB and merge with it. (3) The eastward zonal drift of the EPB on the eastern side slows down while the adjacent EPB on the western side drifts relatively faster and catches up. In one of the cases, a branch of an EPB was observed to get interchanged with another EPB as a result of merging and consequent pinching off from the parent EPB.

1. Introduction

Equatorial plasma bubbles (EPBs) are detrimental for transionospheric radio communication and have been studied for decades (see review articles by *Makela* [2006], *Woodman* [2009], and *Abdu* [2012], and references therein). It is now understood that EPBs form due to generalized Rayleigh-Taylor instability mechanism occurring in the nocturnal ionosphere. On occasions, EPBs grow to reach altitudes of ~1500 km over the dip equator [*Mendillo and Tyler*, 1983; *Shiokawa et al*., 2004]. Though substantial progress has been made in our understanding of their origins, the exact triggering mechanisms are still being debated. Apart from the onset of EPBs, understanding their evolution is also important. It was reported earlier that individual EPBs undergo bifurcations on occasions resulting in Y-shaped EPBs [*Zalesak et al*., 1982; *Mendillo and Tyler*, 1983; *Aggson et al*., 1996; *Yokoyama et al*., 2014]. Sometimes, secondary instabilities forming near the walls of the EPBs give rise to smaller-scale branching and finger-like structures in and around the envelope of the EPBs [*Tsunoda*, 1983; *Makela et al*., 2006]. There have been reports revealing different directions of vertical plasma drift at different altitudes indicating pinching of the EPBs [*Laakso et al*., 1994]. On occasions, the EPBs were seen to shrink in their altitudinal extent over the dip equator [*Narayanan et al*., 2016].

EPBs can serve as tools for studying the nocturnal ionospheric electrodynamics as well. For example, EPBs are used to measure the nocturnal zonal plasma drift in the low-latitude regions [*Martinis et al*., 2003; *Arruda et al*., 2006; *Paulino et al*., 2011; *Chapagain et al*., 2012]. *Martinis et al*. [2003] used airglow imaging observations from two locations to understand the latitudinal variabilities in nocturnal plasma drift. On the other hand, *Chapagain et al*. [2012] use EPB measurements to identify vertical shears in the zonal plasma drift. Such shears are believed to cause tilt of the bubbles, and earlier works support this view [*Zalesak et al*., 1982; *Sekar and Kelley*, 1998; *Sekar et al*., 2012]. However, direct observations of vertical profiles of zonal plasma drift are sparse except for some reports based on Jicamarca radar measurements [*Fejer et al*., 1985; *Hui and Fejer*, 2015].

Recent observations made by Communication and Navigation Outages Forecasting System satellite during extended solar minimum period of 2008–2009 have revealed the existence of plasma depletions of scale sizes ~700 km or more in their longitudinal extent. Such features are referred to as wide plasma bubbles by *Huang et al*. [2011]. On some occasions, even larger-scale depletions with sizes greater than 3500 km are found and are termed as broad plasma depletions. These features frequently occurred during postmidnight hours [*Huang et al*., 2011, 2012]. *Huang et al*. [2011] hypothesized that it is possible for the individual EPBs to merge and consequently produce wide and broad plasma depletions. The simulations of *Huang et al*. [2012] indicated that during the evolution of EPBs, the tilt of one EPB might interfere with the growing channel of the adjacent EPB thereby resulting in their merging. To our knowledge, merging was first observed by *Rohrbaugh et al*. [1989], though was not discussed in detail. Recently, *Huba et al*. [2015] simulated the merging of EPBs and also

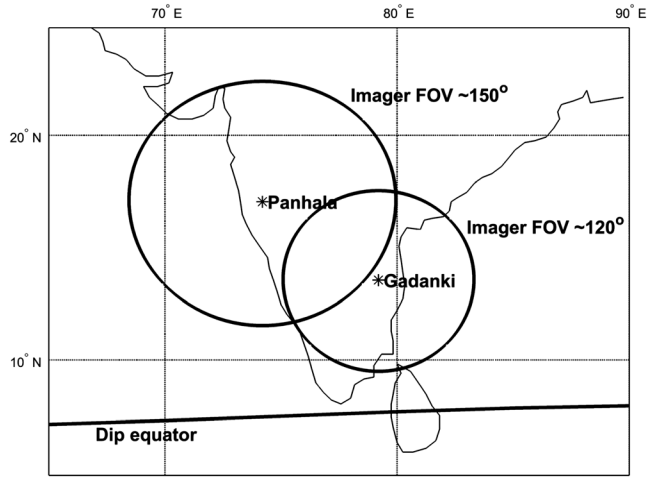

Figure 1. Schematic of observation locations, area covered by images at 250 km altitude, and location of the dip equator.

presented all-sky images in support of their simulations. Their simulations revealed that the electrostatic potentials of adjacent bubbles reconnected favoring the merging.

The plasma depletions spreading over a few degrees in longitude are expected to bring about large-scale variations in the horizontal plasma distribution of postdawn ionosphere, whose effects need to be studied in detail. Certainly, the decay due to cross-field plasma diffusion [*Singh et al*., 1997] will take much longer durations for such broad depletions. Depending on the topside altitude attained by the bubbles over the equator, their refilling duration due to photoionization after sunrise will be larger [*Sidorova and Filippov*, 2014]. Such broad depletions might have important consequences for early morning ionospheric processes because the field line-integrated conductivity is supposedly lower in the region of few to several degrees of longitudes, where the merging of individual EPBs on previous night would have resulted in a broad plasma depletion. Therefore, understanding how individual bubbles merge becomes important.

In this work, based on low-latitude imaging of OI 630.0 nm airglow, we show three different mechanisms by which EPBs undergo merging. Direct observations supporting the simulations of *Huang et al*. [2012] (different tilts between adjacent EPBs bring about merging) are presented for the first time. We also report an example of merging similar to that shown in *Huba et al*. [2015], wherein a branch of one EPB merged with the adjacent EPB. Moreover, a new mechanism for merging of EPBs is proposed based on the observations, in which one EPB slowed in its zonal drift speed and then merged with the trailing EPB. These observations reveal that merging of EPBs is facilitated by multiple pathways. The observations reported herein are made over two different low-latitude sites from the Indian sector, as described in the next section. After briefly describing the database used, we present the results from observations on 6 January 2008, 3 February 2008, 5 February 2008, and 23 March 2009 as separate cases showing the merging of individual EPBs and discuss the implications of these observations.

2. Database

Airglow imaging observations were made with an all-sky airglow imager in manual operation mode from the Indian sector between the years 2007 and 2010, after which the operation was automated. The instrument comprises a six-position filter wheel to observe both mesospheric and thermospheric emissions. The details of the instrument, observation routines, and the basic data analysis techniques employed here can be found in *Narayanan et al*. [2009, 2012, 2013]. The manual observation routine usually involved acquisition of a few successive images of a particular filter for a prolonged duration depending on whether any interesting features were observed in that emission. In this work, we discuss observations made with OI 630.0 nm airglow emission. In addition to the equidistance projection of images over the geographical grid, we have also calculated the apex altitudes over the dip equator corresponding to the footprint of magnetic field lines at 250 km altitude for the area covered by the field of view of the instrument based on the method described in *Chapagain et al*. [2012] and followed in *Narayanan et al*. [2016]. The results discussed herein are based on the observations from Panhala (16.8°N, 74.1°E; 11.1°N dip latitude) on 6 January 2008 and 3 and 5 February 2008 and those from Gadanki (13.5°N, 79.2°E; 6.5°N dip latitude) on 23 March 2009. The apex altitudes are calculated for 74°E longitude for observations from Panhala and 79°E longitude for observations from Gadanki. In order to prevent excess vehicular light from nearby road entering the field of view (FOV), we physically restricted the FOV of the imager to 120° over Gadanki [*Narayanan et al*., 2012]. Figure 1 shows the

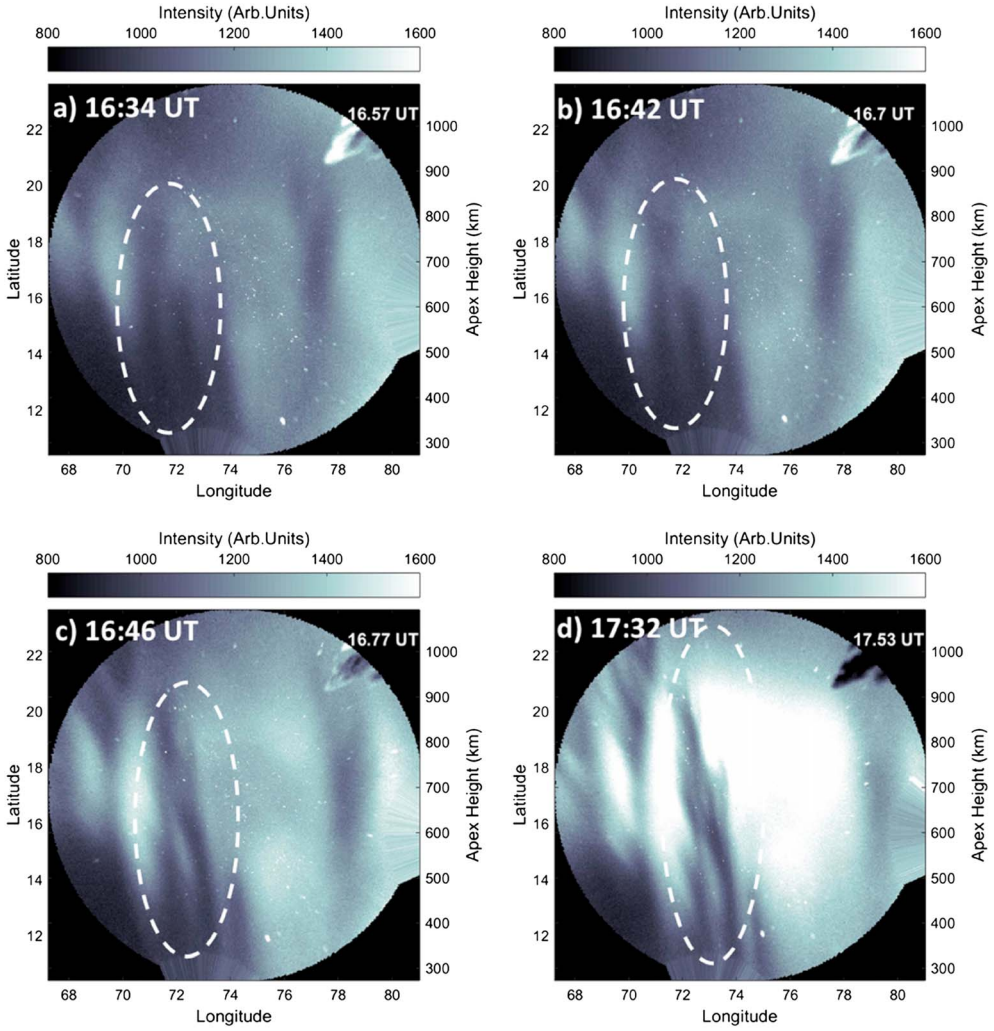

Figure 2. OI 630.0 nm images from Panhala on 6 January 2008. Top and right corresponds to the north and the east, respectively.

schematic of the observation locations, position of the dip equator, and the area covered by the imaging of OI 630.0 nm nightglow for an emission altitude of 250 km.

3. Results

Figure 2 shows the images acquired during the night of 6 January 2008 from Panhala. Attention may be paid to the region marked by dashed ellipses. In Figures 2a and 2b, two closely spaced EPBs in their growth phase can be noticed. From Figure 2c, it is clear that they merged at higher apex altitudes of ~650 km and above. An important feature noticed in this process of merging is the enhanced westward tilt around apex altitudes of 500–600 km on the EPB situated on the right side within the dashed ellipse. This westward tilt enables the EPB channel to evolve into the spatial region of the adjacent EPB, with the end result being the merging of both depleted channels (shown in Figures 2c and 2d).

Figure 3 shows the observations made from Panhala on the night of 3 February 2008. As in Figure 2, the region marked by a dashed ellipse shows the merging. From the marked region in Figures 3a and 3b, it may be noticed that the EPB on the right side develops some finger-like branches on its wall. These branches reach the EPB on the left side by ~15:14 UT, resulting in merging as represented by the arrows in Figure 3c. Two branches of the EPB on the right side appear to merge with the EPB on the left. This observation is similar in nature to that shown in *Huba et al*. [2015]. At the same time, in Figure 3c it may be seen that the channel of

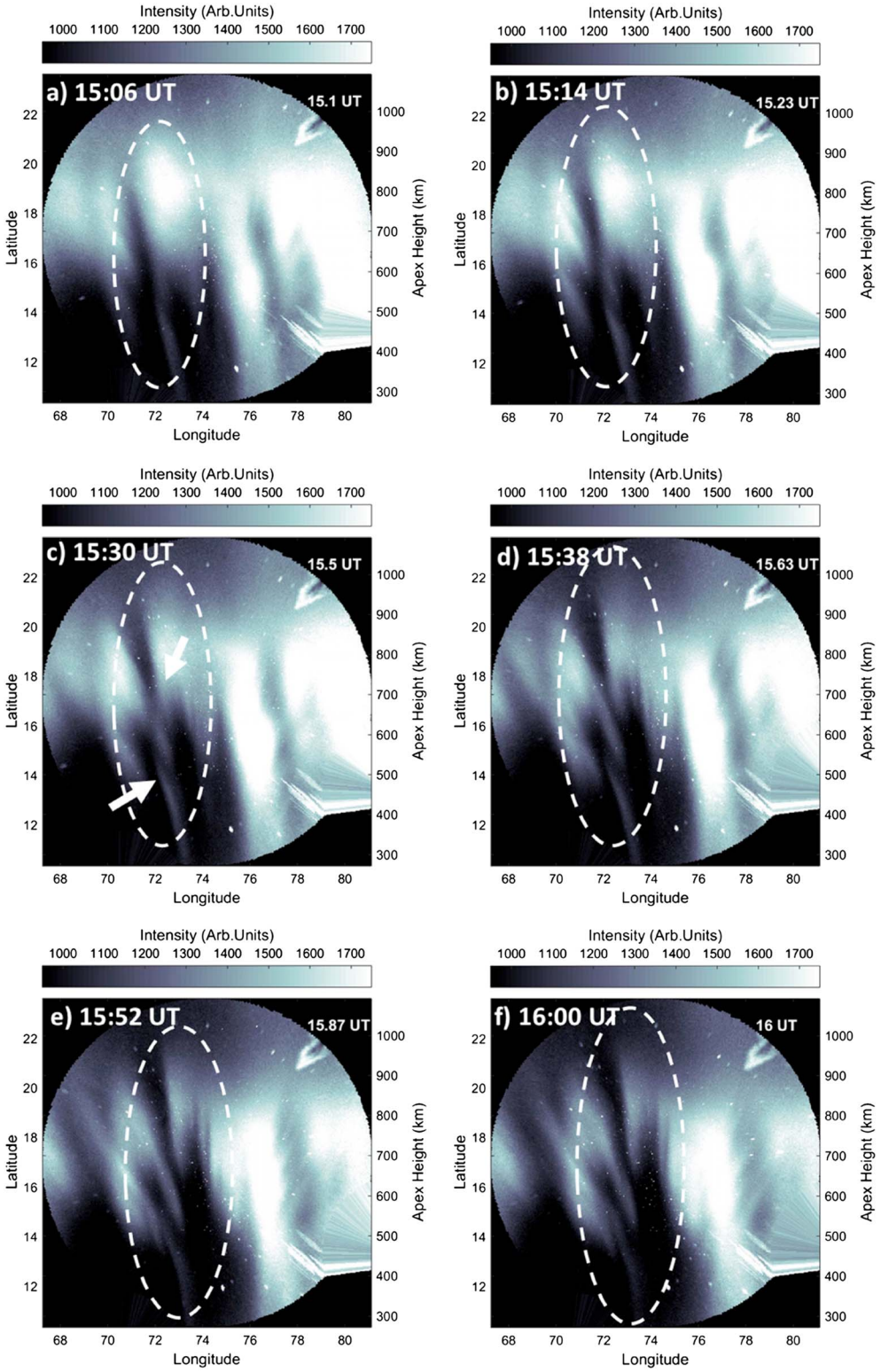

Figure 3. OI 630.0 nm images from Panhala on 3 February 2008.

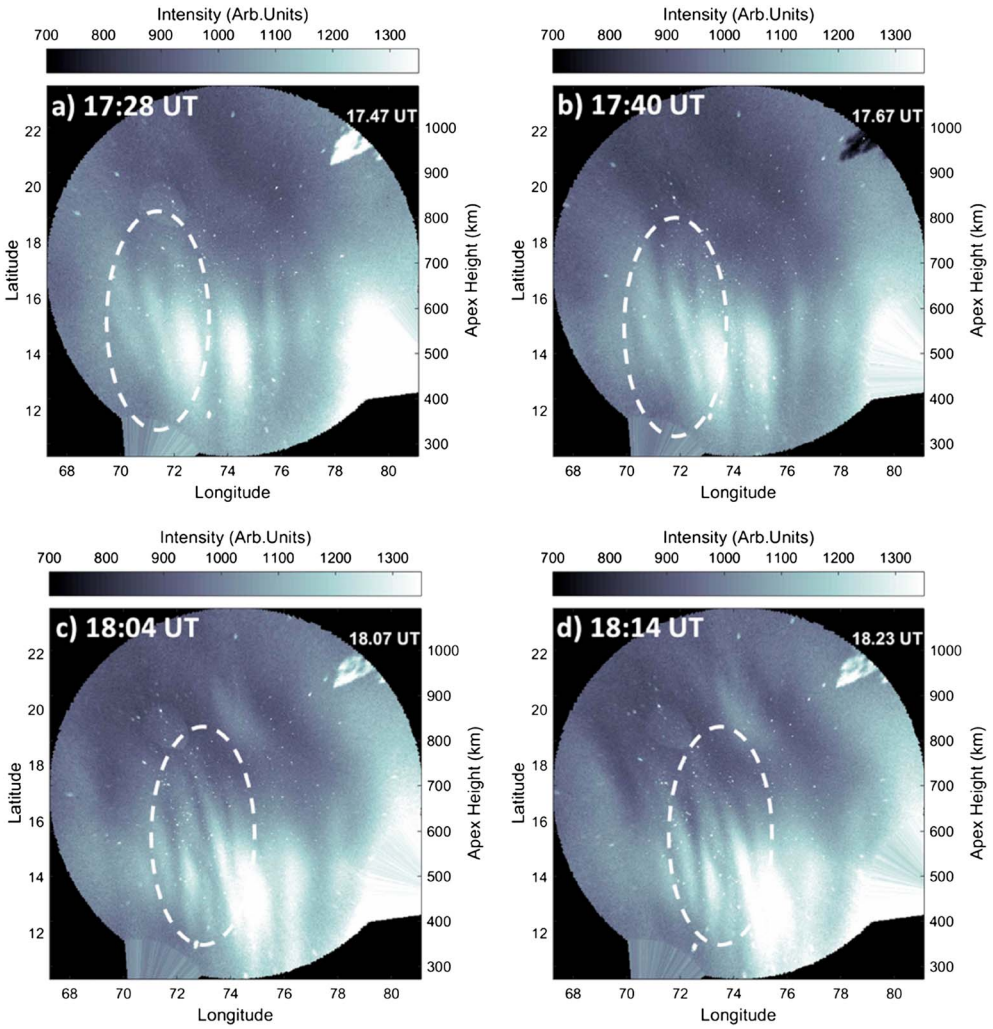

Figure 4. OI 630.0 nm images from Panhala on 5 February 2008.

the EPB on the left edge of the marked portion shows an eastward tilt between apex altitudes of about 550 and 650 km, slightly below the region of merging with one of the branches of EPB on the right. In Figure 3d (at 15:38 UT), that particular part seems to get pinched off from its parent EPB on the left side. Earlier, pinching was reported using satellite observations by *Laakso et al*. [1994] and in the simulations of *Yokoyama et al*. [2014]. Understanding the exact mechanism of the pinching is not the focus of the present work. An interesting point relevant to this study is that the pinched part moves with the EPB on the right side after merging. As a result, what we have noticed is that a part of the EPB on the left side has got pinched off, merged with the EPB on the right to finally become part of the latter. This is a good example of complex interactions between EPBs involving merging.

Figure 4 shows images from the night of 5 February 2008. One can notice the occurrence of many thin EPBs whose lateral dimensions are less than ~50 km in longitudinal extent. Note that they cannot be bifurcation branches of a large EPB because we could trace them from an apex altitude of ~280 km, which is too low for bifurcations to occur. It is a general understanding that bifurcations occur when the EPBs reach topside ionosphere [*Zalesak et al*., 1982; *Aggson et al*., 1996; *Yokoyama et al*., 2014; *Huba et al*., 2015].

We now proceed to examine closely the two EPBs that could be identified within the marked portion in Figure 4a. The second EPB from the right within the dashed ellipse shows an excessive westward tilt compared to the other EPBs on the image. In Figure 4b, the formation of two additional EPBs westward (on the left side) of the existing ones may be noticed in spite of the fact that their intensities were weaker. Those faint

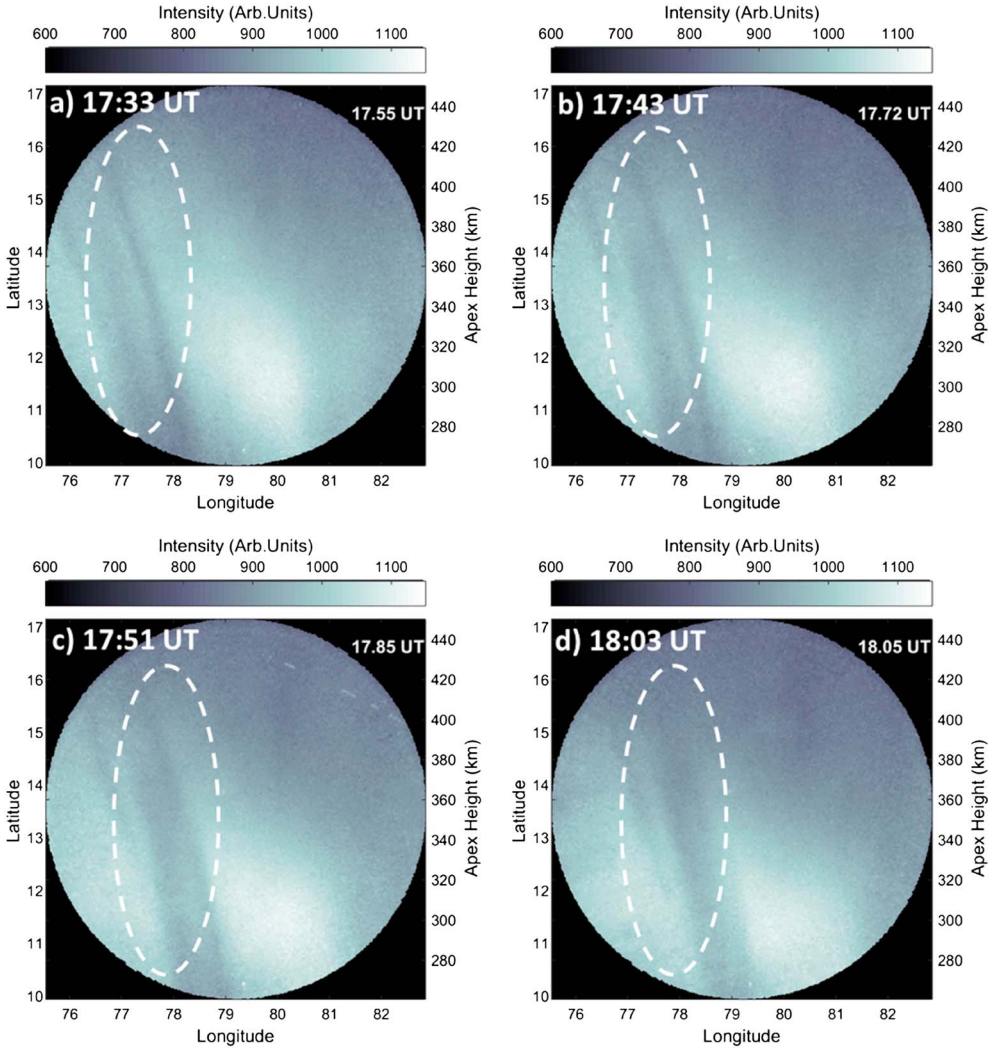

Figure 5. OI 630.0 nm images from Gadanki on 23 March 2009.

EPBs are seen to be relatively well developed in Figures 4c and 4d. From these latter images, it is evident that those EPBs eventually got merged with the tilted EPB. This event also indicates that highly tilted EPB favors merging of growing EPBs from the adjacent areas. It may also be noted that this event was similar to the one presented in Figure 2.

Figure 5 shows another set of images recorded from Gadanki on 23 March 2009. Several aspects of the EPBs observed on this night were already reported in *Narayanan et al*. [2012]. In this work, we focus only on the merging aspect of the EPBs observed on this night that was not discussed in *Narayanan et al*. [2012]. Figure 5a shows three EPBs with considerable westward tilts. This group of EPBs started to enter the FOV of imager from ~17:02 UT. In Figure 5b corresponding to the time 17:43 UT, it may be noticed that the separation distance between the first two EPBs was smaller compared to that seen at the earlier time of 17:33 UT (Figure 5a). Figures 5c and 5d reveal that the first two EPBs have merged. Here it does not seem to be caused by the different tilts as in Figures 2 and 4. Indeed, the figures reveal nearly equal tilts for both EPBs. This case appears to be different from that in Figure 3 as well in which secondary instabilities favored the merging.

4. Discussion

An important aspect to note in the observations shown in Figures 2 and 4 is that the tilts were not uniform between the adjacent EPBs and there was also a height variation in the tilt of an EPB. That is, the tilt at an apex

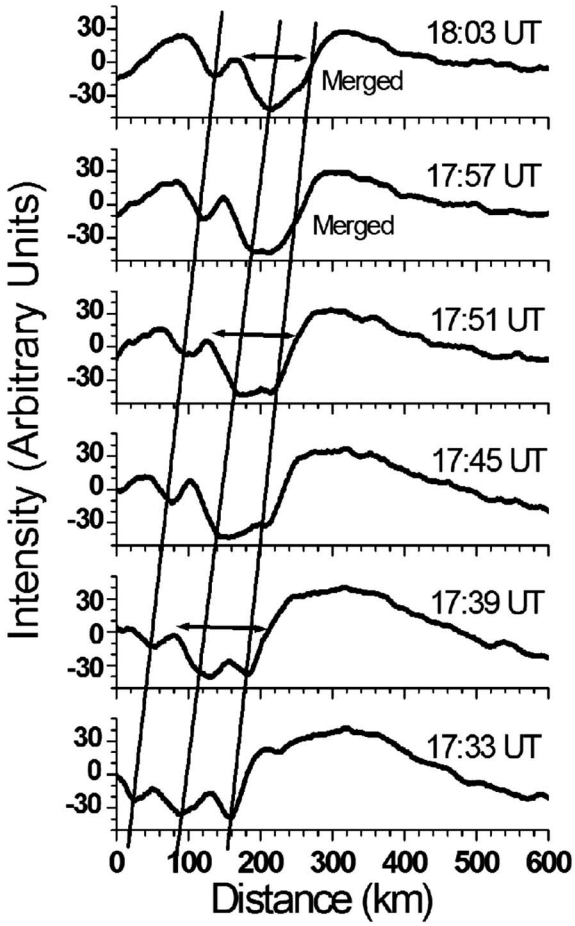

Figure 6. East-west cross sections across the zenith of images obtained on 23 March 2009 from Gadanki.

altitude of 300 km was not the same as that corresponding to 500 km. This nonuniform tilt with altitude facilitates the merging of adjacent EPB channels. Therefore, the observations in Figures 2 and 4 support the simulation results of *Huang et al*. [2012], wherein they found similar nonuniform tilting of an EPB leading to merging with adjacent EPBs.

The westward tilt of EPBs is attributed to the altitudinal shear in zonal plasma drift. The zonal plasma drifts in the equatorial region are associated with thermospheric zonal winds and the ratio of integrated conductivities in the equatorial *F* region and off equatorial *F* and *E* regions along the field line [*Anderson and Mendillo*, 1983; *Zalesak et al*., 1982; *Mendillo and Tyler*, 1983; *Sinha and Raizada*, 2000]. Our observations indicate that it is possible for the zonal plasma drifts to vary with altitude over the dip equator and this variation is not uniform in longitudinal extent over a few degrees, at least on certain occasions. Indeed, the zonal plasma drift speeds appear to vary within a distance of ~100 km (i.e., 1° longitude) enabling adjacent EPBs with thickness of ~50 km merge with each other. These observations also imply that the altitudinal profile of zonal plasma drifts can vary within few minutes. The cause for the variation of plasma drifts within such short spatiotemporal scales is not known at present. Nevertheless, the observations of zonal plasma drifts presented in *Fejer et al*. [1985] indicate that there is noticeable difference in the altitudinal profile of zonal plasma drifts within few minutes [see *Fejer et al*., 1985, Figure 5]. Our observations indicate that the existence of short spatiotemporal variabilities in the zonal plasma drifts similar to those presented in *Fejer et al*. [1985] would have caused the merging in the examples shown in Figures 2 and 4. Higher-resolution measurements of thermospheric and ionospheric parameters might reveal better insight about this aspect.

The example shown in Figure 3 involves merging of EPBs, wherein we invoke a different mechanism to explain the feature. On 3 February 2008 (see Figure 3), the EPBs evolved with finger-like structures on their edges that are usually attributed to secondary instabilities. Secondary instabilities are known to occur on the walls of plasma bubbles when conditions are favorable. For example, wind-driven secondary instabilities occur when the neutral wind blows antiparallel to the plasma density gradient with geomagnetic field directed perpendicular to both the neutral wind component and the plasma density gradient [*Tsunoda*, 1983; *Makela et al*., 2006]. The nocturnal thermospheric zonal winds are usually eastward [*Emmert et al*., 2006], and the plasma density gradients in the western wall of EPBs are westward. Thus, the western wall is more favorable for onset of wind-driven secondary instabilities. Observation of finger-like branches is not an unusual feature noticed in all-sky images. In the present case, two of the branches from the western wall of the EPB located on the right side evolved and then went through a merging with the EPB on the left side (see Figure 3). We thus have a scenario wherein secondary instabilities facilitate branching of EPBs on their walls. Some of the branches reach out to the adjacent EPBs and merge.

The nature of the merging in the example shown in Figure 5 is different from both the mechanisms described above. In order to understand better the merging process in this case, we present the detrended east-west cross sections of the images from the overhead sky (corresponding to zenith) in Figure 6. The curves clearly reveal three EPBs in the beginning (the sharp decrease in intensity implies the presence of an EPB). With the passage of time, only two EPB signatures are discernable (see the panels corresponding to 17:57 UT and 18:03 UT in Figure 6). The rightmost EPB noticed at earlier times (17:33 UT and 17:39 UT) is not seen at later times (in panels corresponding to 17:57 and 18:03 UT) since by then the same has merged with the adjacent EPB (see Figure 5 as well).

In Figure 6, we have drawn three lines corresponding to the deepest points of the EPBs. The line corresponding to the rightmost EPB from the earlier time of 17:33 UT is extended through the two panels in the top, though this signature is not present therein. This is done in order to show the convergence between the lines joining the location of first (right) and second (middle) EPBs. The inference is that as the first EPB slows down and the adjacent EPB catches up with it leading to the merging of the two bubbles.

The estimated drift speed of the first EPB during the first half hour of observations between 17:02 and 17:33 UT was ~86 m/s eastward (not shown here but may be noted from Figure 5 of *Narayanan et al*. [2012]). This speed got reduced to ~55 m/s by 17:51 UT, the time of initiation of the merging. The drift speed of the second (middle) and third (left) EPBs was approximately 66 m/s and 57 m/s, respectively, within the observed duration. The percentage errors in the drift speed estimations are typically ~15% or less. The estimated drift speeds support our finding that the leading EPB slowed down favoring a merging of the relatively fast moving trailing EPB with the leading one. These aspects are also indicated by the double-headed arrows drawn on the panels corresponding to 17:39, 17:51, and 18:03 UT. The arrows give the distance between the eastern edge of the first EPB and the western edge of the second EPB. The arrow length representing the combined spatial extent of the two EPBs was larger before the EPBs merged (see the panel corresponding to 17:39 UT) and the spatial extent decreased as the EPBs merged at subsequent times (see the panels for 17:51 and 18:03 UT).

This process wherein the leading EPB slows down and the trailing EPB catches up with it resulting in merging is a new mechanism, hitherto not reported, proposed herein to explain the merging of two individual EPBs. It is known that the drift speeds of EPBs decrease with time during the night [e.g., *Martinis et al*., 2003]. There were even reports that EPBs change their drift direction from east to west during the postmidnight hours and during magnetically disturbed conditions [*Paulino et al*., 2010]. Any merging of adjacent EPBs occurring during such periods can be explained by this mechanism. For example, if at a particular local time the drift changes from eastward to westward, then the leading EPB will start drifting westward, while the adjacent trailing EPB will still be moving eastward and it is then expected that the latter would merge with the leading EPB. Further, such a mechanism can also explain the presence of plasma depletions on certain occasions with widths much larger than those of EPBs occurring during other times.

5. Summary and Conclusions

We have described four cases of merging of EPBs in this work. Based on the results obtained, we invoke three different mechanisms. In two of the cases, individual EPBs merge when one of the EPBs develops an excessive tilt and reaches the adjacent EPB. This suggestion was earlier made by *Huang et al*. [2012] through their simulation studies. We provide herein the first observational evidence for this kind of merging earlier seen in simulations. Another feature that was revealed in this study is to do with the merging between adjacent EPBs caused by the formation of secondary instabilities growing on the western wall of the EPBs. In the same example, we found a complex interaction between the adjacent EPBs, wherein a part of one of the EPBs gets pinched off and becomes a part of the adjacent EPB due to merging phenomenon. The other mechanism that seems to account for the merging observed on certain other occasions involves the slowing down of the leading EPB on the eastern side, while the trailing one subsequently catches up with it. This is a viable mechanism involving merging of multiple EPBs that can explain the presence of wide and broad plasma depletions.

To conclude, as EPBs play a prominent role in undermining the utility of communication and navigation systems, understanding of the merging of the EPBs under various conditions is important to comprehend the different phases of their evolution. Further, the aftereffects of wide and broad plasma depletions that result from merging need to be studied in detail.

Acknowledgments

The data used in this work were collected by Indian Institute of Geomagnetism (IIG) with the support from the Department of Science and Technology, Government of India. The data can be accessed by contacting S. Gurubaran (IIG). The lead author V.L.N. thanks the support provided by the Department of Science and Technology, Government of India, under the INSPIRE Faculty Scheme (grant DST/INSPIRE/04/2014/001636). This work was partly supported by JSPS KAKENHI grant 15H05815. The assistance rendered by P.T. Patil and A.K. Patra in conducting the campaigns at Panhala and Gadanki, respectively, is gratefully acknowledged. We thank K. Emperumal for his help in the installation of the instrument at the campaign sites. The IGRF-11 model used to calculate apex altitudes was obtained from IAGA workgroup V-MOD.

References

Abdu, M. A. (2012), Equatorial spread *F* development and quiet time variability under solar minimum conditions, *Indian J. Radio Space Phys.*, *41*, 168–183.

Aggson, T. L., H. Laakso, N. C. Maynard, and R. F. Pfaff (1996), In situ observations of bifurcation of equatorial ionospheric plasma depletions, *J. Geophys. Res.*, *101*, 5125–5132, doi:10.1029/95JA03837.

Anderson, D. N., and M. Mendillo (1983), Ionospheric conditions affecting the evolution of equatorial plasma depletions, *Geophys. Res. Lett.*, *10*, 541–544, doi:10.1029/GL010i007p00541.

Arruda, D. C. S., J. H. A. Sobral, M. A. Abdu, V. M. Castilho, H. Takahashi, A. F. Medeiros, and R. A. Buriti (2006), Theoretical and experimental zonal drift velocities of the ionospheric plasma bubbles over the Brazilian region, *Adv. Space Res.*, *38*, 2610–2614, doi:10.1016/j.asr.2006.05.015.

Chapagain, N. P., M. J. Taylor, J. J. Makela, and T. M. Duly (2012), Equatorial plasma bubble zonal velocity using 630.0 nm airglow observations and plasma drift modeling over Ascension Island, *J. Geophys. Res.*, *117*, A06316, doi:10.1029/2012JA017750.

Emmert, J. T., M. L. Faivre, G. Hernandez, M. J. Jarvis, J. W. Meriwether, R. J. Niciejewski, D. P. Sipler, and C. A. Tepley (2006), Climatologies of nighttime upper thermospheric winds measured by ground-based Fabry-Perot interferometers during geomagnetically quiet conditions: 1. Local time, latitudinal, seasonal, and solar cycle dependence, *J. Geophys. Res.*, *111*, A12302, doi:10.1029/2006JA011948.

Fejer, B. G., E. Kudeki, and D. T. Farley (1985), Equatorial *F* region zonal plasma drifts, *J. Geophys. Res.*, *90*, 12,249–12,255, doi:10.1029/JA090iA12p12249.

Huang, C.-. S., O. de La Beaujardiere, P. A. Roddy, D. E. Hunton, R. F. Pfaff, C. E. Valladares, and J. O. Ballenthin (2011), Evolution of equatorial ionospheric plasma bubbles and formation of broad plasma depletions measured by the C/NOFS satellite during deep solar minimum, *J. Geophys. Res.*, *116*, A03309, doi:10.1029/2010JA015982.

Huang, C.-S., J. M. Retterer, O. de La Beaujardiere, P. A. Roddy, D. E. Hunton, J. O. Ballenthin, and R. F. Pfaff (2012), Observations and simulations of formation of broad plasma depletions through merging process, *J. Geophys. Res.*, *117*, A02314, doi:10.1029/2011JA017084.

Huba, J. D., T.-W. Wu, and J. J. Makela (2015), Electrostatic reconnection in the ionosphere, *Geophys. Res. Lett.*, *42*, 1626–1631, doi:10.1002/2015GL063187.

Hui, D., and B. G. Fejer (2015), Daytime plasma drifts in the equatorial lower ionosphere, *J. Geophys. Res. Space Physics*, *120*, 9738–9747, doi:10.1002/2015JA021838.

Laakso, H., T. L. Aggson, R. F. Pfaff, and W. B. Hanson (1994), Downdrafting plasma flow in equatorial bubbles, *J. Geophys. Res.*, *99*, 11,507–11,515, doi:10.1029/93JA03169.

Makela, J. J. (2006), A review of imaging low-latitude ionospheric irregularity process, *J. Atmos. Sol. Terr. Phys.*, *68*, 1441–1458, doi:10.1016/j.jastp.2005.04.014.

Makela, J. J., M. C. Kelley, and M. J. Nicolls (2006), Optical observations of the development of secondary instabilities on the eastern wall of an equatorial plasma bubble, *J. Geophys. Res.*, *111*, A09311, doi:10.1029/2006JA011646.

Martinis, C., J. V. Eccles, J. Baumgardner, J. Manzano, and M. Mendillo (2003), Latitude dependence of zonal plasma drifts obtained from dual-site airglow observations, *J. Geophys. Res.*, *108*(A3), 1129, doi:10.1029/2002JA009462.

Mendillo, M., and A. Tyler (1983), Geometry of depleted plasma regions in the equatorial ionosphere, *J. Geophys. Res.*, *88*, 5778–5782, doi:10.1029/JA088iA07p05778.

Narayanan, V. L., S. Gurubaran, and K. Emperumal (2009), Imaging observations of upper mesospheric nightglow emissions from Tirunelveli (8.7°N), *Indian J. Radio Space Phys.*, *38*, 150–158.

Narayanan, V. L., A. Taori, A. K. Patra, K. Emperumal, and S. Gurubaran (2012), On the importance of wave-like structures in the occurrence of equatorial plasma bubbles: A case study, *J. Geophys. Res.*, *117*, A01306, doi:10.1029/2011JA017054.

Narayanan, V. L., S. Gurubaran, K. Emperumal, and P. T. Patil (2013), A study on the nighttime equatorward movement of ionization anomaly using thermospheric airglow imaging technique, *J. Atmos. Sol. Terr. Phys.*, *103*, 113–120, doi:10.1016/j.jastp.2013.03.028.

Narayanan, V. L., S. Gurubaran, K. Shiokawa, and K. Emperumal (2016), Shrinking equatorial plasma bubbles, *J. Geophys. Res. Space Physics*, *121*, doi:10.1002/2016JA022633.

Paulino, I., A. F. Medeiros, R. A. Buriti, J. H. A. Sobral, H. Takahashi, and D. Gobbi (2010), Optical observations of plasma bubble westward drifts over Brazilian tropical region, *J. Atmos. Sol. Terr. Phys.*, *72*, 521–527, doi:10.1016/j.jastp.2010.01.015.

Paulino, I., A. F. Medeiros, R. A. Buriti, H. Takahashi, J. H. A. Sobral, and D. Gobbi (2011), Plasma bubble zonal drift characteristics observed by airglow images over Brazilian tropical region, *Rev. Bras. Geof.*, *29*, 239–246, doi:10.1590/S0102-261X2011000200003.

Rohrbaugh, R. P., W. B. Hanson, B. A. Tinsley, B. L. Cragin, J. P. McClure, and A. L. Broadfoot (1989), Images of transequatorial bubbles based on field-aligned airglow observations from Haleakala in 1984–1986, *J. Geophys. Res.*, *94*, 6763–6770, doi:10.1029/JA094iA06p06763.

Sekar, R., and M. C. Kelley (1998), On the combined effects of vertical shear and zonal electric field patterns on nonlinear equatorial spread *F* evolution, *J. Geophys. Res.*, *103*, 20,735–20,747, doi:10.1029/98JA01561.

Sekar, R., D. Chakrabarty, and D. Pallamraju (2012), Optical signature of shear in the zonal plasma flow along with a tilted structure associated with equatorial spread *F* during a space weather event, *J. Atmos. Sol. Terr. Phys.*, *75–76*, 57–63, doi:10.1016/j.jastp.2011.05.009.

Shiokawa, K., Y. Otsuka, T. Ogawa, and P. Wilkinson (2004), Time evolution of high-altitude plasma bubbles imaged at geomagnetic conjugate points, *Ann. Geophys.*, *22*, 3137–3143, doi:10.5194/angeo-22-3137-2004.

Sidorova, L. N., and S. V. Filippov (2014), Plasma bubbles in the topside ionosphere: Estimations of the survival possibility, *J. Atmos. Sol. Terr. Phys.*, *119*, 35–41, doi:10.1016/j.jastp.2014.06.013.

Singh, S., D. K. Bamgboye, J. P. McClure, and F. S. Johnson (1997), Morphology of equatorial plasma bubbles, *J. Geophys. Res.*, *102*, 20,019–20,029, doi:10.1029/97JA01724.

Sinha, H. S. S., and S. Raizada (2000), Some new features of ionospheric plasma depletions over the Indian zone using all sky optical imaging, *Earth Planets Space*, *52*, 549–559, doi:10.1186/BF03351662.

Tsunoda, R. T. (1983), On the generation and growth of equatorial backscatter plumes: 2. Structuring of the west walls of upwellings, *J. Geophys. Res.*, *88*, 4869–4874, doi:10.1029/JA088iA06p04869.

Woodman, R. F. (2009), Spread *F*—An old equatorial aeronomy problem finally resolved?, *Ann. Geophys.*, *27*, 1915–1934, doi:10.5194/angeo-27-1915-2009.

Yokoyama, T., H. Shinagawa, and H. Jin (2014), Nonlinear growth, bifurcation, and pinching of equatorial plasma bubble simulated by three-dimensional high-resolution bubble model, *J. Geophys. Res. Space Physics*, *119*, 10,474–10,482, doi:10.1002/2014JA020708.

Zalesak, S. T., S. L. Ossakow, and P. K. Chaturvedi (1982), Nonlinear equatorial spread *F*: The effect of neutral winds and background Pedersen conductivity, *J. Geophys. Res.*, *87*, 151–166, doi:10.1029/JA087iA01p00151.